ADVANCED ELECTRONIC MATERIALS Open Access
www.advelectronicmat.de

Highly Efficient and Flexible Thin Film Thermoelectric Materials from Blends of PEDOT:PSS and $AgSb_{0.94}Cd_{0.06}Te_2$

Mahima Goel, Adrian Hochgesang, Animesh Bhui, Kanishka Biswas, and Mukundan Thelakkat**

Mechanically stable and flexible composite TE thin films based on PEDOT:PSS and $AgSb_{0.94}Cd_{0.06}Te_2$ blend by hot pressing on porous PVDF substrate are fabricated. A considerable enhancement of S and σ is observed in the regime of 60–97.5 wt.% of $AgSb_{0.94}Cd_{0.06}Te_2$. High Seebeck coefficients of up to 204.9 µV K^{-1} and a high-power factor of 53.45 µW m^{-1} K^{-2} are obtained for 97.5 wt.% of $AgSb_{0.94}Cd_{0.06}Te_2$ content. However, there is a decrease in electrical conductivity on bending or storage under air. No loss of mechanical integrity can be detected in the SEM of bent films. Ultraviolet photoelectron spectroscopy reveals that overall energy levels of composite systems are either similar to PEDOT:PSS ($\varphi = 5.00 \pm 0.16$ eV, IP $= 5.12 \pm 0.02$ eV) or $AgSb_{0.94}Cd_{0.06}Te_2$ ($\varphi = 4.43 \pm 0.11$ eV, IP $= 4.57 \pm 0.01$ eV), depending on the blend ratio. Transport mechanisms are studied using Mott–Schottky measurements, and by calculating the weighted charge carrier mobility, which increases continuously up to 5.5 cm^2 V^{-1} s^{-1} for the highest inorganic content. It is demonstrated that a high inorganic content TE composite results in a flexible TE film achieving 80% of the Seebeck value of the pure inorganic component.

1. Introduction

Polymer-based flexible thermoelectric (TE) materials are currently receiving unprecedented attention due to their capability to convert waste heat into electricity using wearable, bendable, and large-area thermoelectric devices. Polymeric materials have advantageously low thermal conductivities, can be easily printed in different shapes and sizes, affording non-conventional TE geometries, and hence are applicable to a large variety of heat sources and surfaces.[1–4] Despite these advantages, the use of polymeric semiconductors in TEs often reaches a limit due to inherently low electrical conductivities (in the range of 10^{-6}–10^{-11} S cm^{-1}) of polymers in undoped states.[5] The low electrical conductivity is unfavorable for high efficiency or figure of merit (ZT) of a TE material, as defined in Equation (1).

$$ZT = \frac{S^2 \sigma T}{\kappa} \tag{1}$$

Here, S is the thermoelectric power or Seebeck coefficient ($S = \Delta V/\Delta T$), ΔV is the voltage difference across a sample under a fixed temperature gradient (ΔT) at a fixed temperature T. σ represents the isothermal electrical conductivity, and κ is the thermal conductivity at temperature T. The factor $S^2\sigma$ is known as the power factor (PF). Considering that κ of polymers is generally very low (0.1–0.2 W m^{-1} K^{-1}), a high PF requires that both electrical conductivity (σ) and Seebeck coefficient (S) of a thermoelectric material must be high or enhanced simultaneously.[6] Therefore, polymeric semiconductors are doped to obtain appreciable electrical conductivities by adding either electron donors (p-doping) or acceptors (n-doping).[7] But, when carrier concentration (n) is increased to enhance electrical conductivity, the Seebeck coefficient decreases to the power of −2/3 of charge carrier concentration in accordance with the Pisarenko relation as described in Equation (2), originally derived for metals or degenerate semiconductors.

$$S = \frac{8\pi^2 k_B^2}{3eh^2} m^* T \left(\frac{\pi}{3n}\right)^{2/3} \tag{2}$$

As a result, doped polymer materials exhibit low thermoelectric efficiencies due to the tradeoff between S and σ upon doping.[8] Therefore, the challenge to create highly efficient polymer-based thermoelectric materials lies in finding new synthetic and materials processing methods to increase the two contradictory properties (S and σ), simultaneously, keeping the thermal conductivity low. This is summarized in the ideal TE material concept of phonon-glass electron-crystal materials, where the phonon-glass requirement satisfies very low lattice thermal conductivity, and the electron-crystal property stems from high electronic parameters (S and σ).[9]

M. Goel, A. Hochgesang, M. Thelakkat
Applied Functional Polymers
University of Bayreuth
Universitätstr. 30, 95447 Bayreuth, Germany
E-mail: mahima.goel@uni-bayreuth.de;
mukundan.thelakkat@uni-bayreuth.de

A. Bhui, K. Biswas
New Chemistry Unit
Jawaharlal Nehru Centre for Advanced Scientific Research
Jakkur, Bangalore, Karnataka 560064, India

The ORCID identification number(s) for the author(s) of this article can be found under https://doi.org/10.1002/aelm.202500118

DOI: 10.1002/aelm.202500118

In the case of polymeric TE materials, there are two main methods to synergize S and σ. The first method makes use of the blending of different polymers, and the second method involves the copolymerization of different donor-acceptor or donor–donor building blocks. For the blending approach, Katz et al. showed that blending poly-(3-hexylthiophene) (P3HT) with 30 wt.% of poly(3-hexylthiothiophene) (P3HTT) increased S and σ simultaneously with increasing doping with tetrafluorotetracyanoquinodimethane (F4TCNQ). In a subsequent study by Katz et al., a similar slight decoupling of S and σ was reported as alkylthio-substituted polythiophene (PQTS12) was used as an additive in poly(bisdodecylquaterthiophene) (PQT12) with (F4TCNQ) and nitrosyl tetrafluoroborate (NOBF4) as dopants.[10,11] Kemerink et al. explained the blending approach by suggesting that blending allows a rational optimization of the Seebeck coefficient through modification of the density of states. For example, when a polymeric semiconductor P3HT having a shallow highest occupied molecular orbital (HOMO) level is mixed with varying fractions of PTB7 and TQ1 having deeper HOMOs to form binary blends, high Seebeck coefficients were obtained while retaining reasonable conductivities by dopeing of F4TCNQ.[12] Yee et al. achieved simultaneous enhancement of σ and S for nickel ethenetetrathiolate (NiETT)polymer and poly(vinylidene fluoride) (PVDF) blend using thermal annealing as a post-treatment process.[13] The second method, the copolymerization approach, was used by Chen et al. in random copolymerization of D-A type (DPP-TT) and electron-rich D-D type (g32T-TT) building blocks to strike a balance between electrical conductivity and Seebeck coefficient.[14] In summary, although a proof of concept was validated in the above reports, limitations such as small doping ranges, poor doping efficiency of the dopants, and only marginal simultaneous improvements in electrical conductivity and Seebeck coefficient remained as unsolved problems.

To overcome the above challenges of pure organic blends and dopants, the polymer TE community has started exploring composites of polymeric semiconductors with high Seebeck inorganic TE materials. In this direction, PEDOT:PSS is one of the most widely used semiconducting polymers for flexible TE applications due to its high σ, low κ, excellent environmental stability, and film-forming properties. Previous studies show that a maximum Seebeck coefficient of 50 $\mu V\ K^{-1}$ is possible when PEDOT:PSS was tested as a thermoelectric material to realize thin film applications.[15,16] By dedoping PEDOT:PSS, a power factor in the range of 100 $\mu W\ K^{-2}$ m was obtained, still the Seebeck coefficient remaining below 50 $\mu V\ K^{-1}$. To increase the Seebeck coefficient further, PEDOT:PSS is combined with high Seebeck inorganic TE semiconductors such as Bi_2Te_3, Sb_2Te_3, SnSe, or $Bi_{0.5}Sb_{1.5}Te_3$.[17,18] Here, the Seebeck coefficient of the inorganic TE material alone varies in a very broad range; the values being ≈520 $\mu V\ K^{-1}$ for SnSe, ≈250 $\mu V\ K^{-1}$ for $Bi_{0.5}Sb_{1.5}Te_3$, ≈180 $\mu V\ K^{-1}$ for Bi_2Te_3, and ≈125 $\mu V\ K^{-1}$ for Sb_2Te_3. The main issue here is that the high Seebeck coefficients (520–125 $\mu V\ K^{-1}$) of the inorganic component could not be significantly manifested in the composites with inorganic content less than 90 wt.%. For example, Zhao et al. reached a power factor of 9.9 $\mu W\ m^{-1}K^{-2}$ in PEDOT:PSS films containing 10 wt.% of Bi_2Te_3, but the Seebeck coefficient varied in a tiny range from 14.2 to 18.6 $\mu V\ K^{-1}$.[19] Wei et al. achieved a higher power factor of 47.7 $\mu W\ m^{-1}\ K^{-2}$ in PEDOT:PSS/PVA/$Bi_{0.5}Sb_{1.5}Te_3$ films containing 36 wt.% of $Bi_{0.5}Sb_{1.5}Te_3$, but the Seebeck coefficient decreased drastically below 50 $\mu V\ K^{-1}$ with increasing content of $Bi_{0.5}Sb_{1.5}Te_3$ above 60 wt.%.[20] On the other hand, Ju et al obtained appreciably good values (S≈200 $\mu V\ K^{-1}$ and PF = 320 $\mu W\ m^{-1}\ K^{-2}$ by blending PEDOT:PSS with 50 wt.% of exfoliated SnSe nanosheets having very high S values (≈560 $\mu V\ K^{-1}$) and low thermal conductivity (≈0.6 $W\ m^{-1}\ K^{-1}$) at 300 K.[18b] Even then, it is very difficult to reach the high S values of the original inorganic component in a composite, and a simultaneous improvement of both S and σ is still elusive.

Another limiting factor is the difficulty in preparing stable, crack-free films with high concentrations of inorganics due to brittleness, voids on the surfaces, delamination, and cracking of the composite films at inorganic content greater than 90%. Even though Wang et al. could overcome issues of cracking and brittleness for composite systems prepared on PTFE film using high content of Cu-doped MgAgSb, graphene and PEDOT:PSS, a maximum power factor of only 16 $\mu W\ m^{-1}\ K^{-2}$ was obtained for the flexible systems.[21]

In the present study, we report our observations on the simultaneous enhancement of S and σ with increasing amounts of $AgSb_{0.94}Cd_{0.06}Te_2$ in dense, crack-free, flexible, and highly efficient PEDOT: PSS/$AgSb_{0.94}Cd_{0.06}Te_2$ composite TE thin films on PVDF substrate in the whole composition regime. The inorganic TE material, $AgSb_{0.94}Cd_{0.06}Te_2$, is itself highly air-stable and exhibits a high Seebeck value in the range of 248 $\mu V\ K^{-1}$ and electrical conductivity of 222 $S\ cm^{-1}$, when measured in a highly densified pellet near room temperature.[22,23,24] Flexible PEDOT: PSS/$AgSb_{0.94}Cd_{0.06}Te_2$ composite thin films containing 0, 30, 50, 90, 95, and 97.5 wt.% of $AgSb_{0.94}Cd_{0.06}Te_2$ were fabricated by blending PEDOT: PSS with $AgSb_{0.94}Cd_{0.06}Te_2$ particles (obtained by grinding synthesized ingots) and, doctor blading the slurry on porous PVDF substrates followed by hot pressing to obtain inorganic-rich blends. To the best of our knowledge, in all the previous studies related to composite thin films based on PEDOT: PSS, composites containing high inorganic content above 90 wt.% were not explored, apparently due to the extreme difficulty in realizing mechanically stable and flexible composite films. Here, we report for the first time PEDOT: PSS/$AgSb_{0.94}Cd_{0.06}Te_2$ thin films leading to highly efficient composite TE materials with S values reaching up to 205$\mu V\ K^{-1}$and the highest power factor of 53.45 $\mu W\ m^{-1}\ K^{-2}$. We demonstrate that the mixing of conducting polymers with highly efficient inorganic TE materials can provide an innovative way to design composite thermoelectric materials with high S and σ values. The primary focus of the work is on the following: i) fabrication of mechanically stable and flexible PEDOT:PSS/$AgSb_{0.94}Cd_{0.06}Te_2$ thin films with high inorganic content by hot pressing, ii) fundamental investigations on the impact of composition, thicknesses, and densification conditions on the morphology, structure, and thermoelectric properties of the composite films and iii) understanding the simultaneous enhancement of S and σ and the transport mechanisms in this composite system by determining the energy levels, charge carrier concentation and weighted charge carrier mobilities of individual materials and the composite systems.

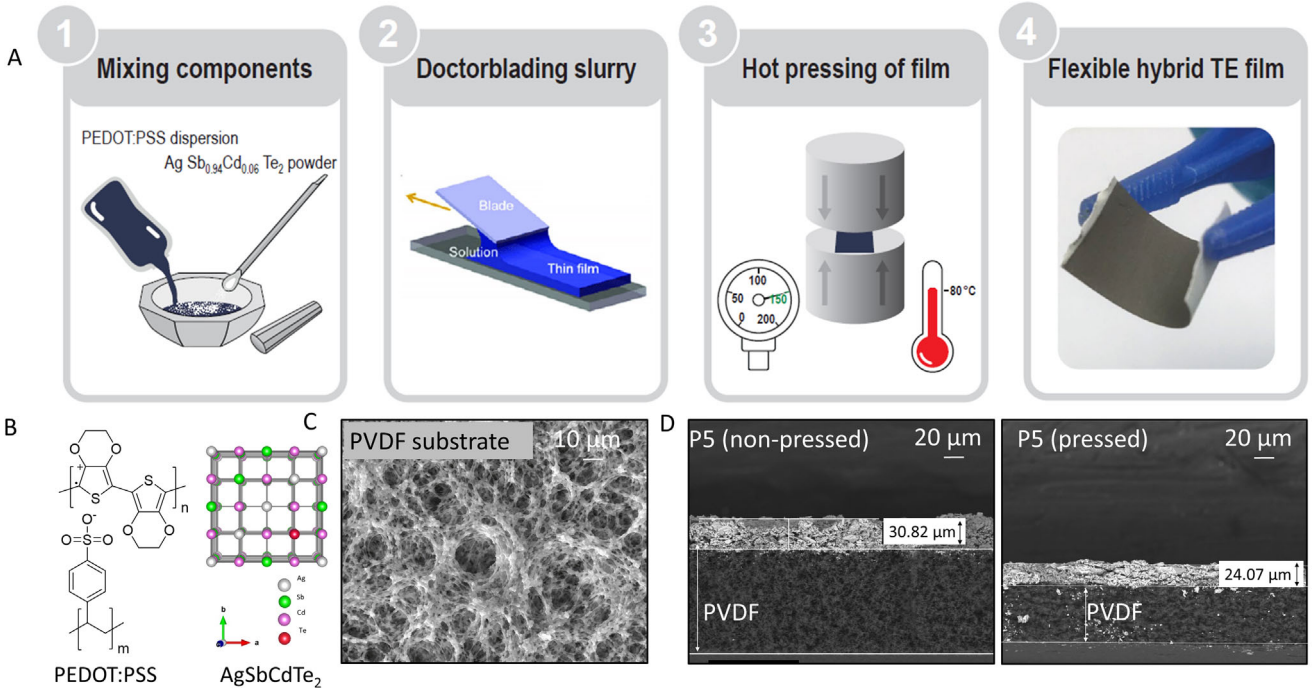

Figure 1. A) Sketch of processing steps (1–4) involved in fabricating flexible composite TE thin films; B) The chemical structure of PEDOT: PSS and crystal structure of $AgSbCdTe_2$ 24; C) Surface SEM image of PVDF substrate; D) Cross sectional SEM images of non-pressed P5 sample (left) and hot-presseed P5 (right).

2. Results and Discussions

2.1. Fabrication of Flexible PEDOT: PSS/$AgSb_{0.94}Cd_{0.06}Te_2$ Composite Thin Films

The fabrication process of PEDOT:PSS/$AgSb_{0.94}Cd_{0.06}Te_2$ composite thin films is schematically shown in **Figure 1**. PEDOT:PSS dispersion and $AgSb_{0.94}Cd_{0.06}Te_2$ powder were transferred to a mortar and mixed well with the help of a pestle to obtain a thick slurry. Using a thick Kapton foil, the slurry was uniformly doctor bladed on the PVDF membrane substrates as schematically represented in steps 1 and 2 of Figure 1. For composite compositions, containing 50 wt.% or lower amounts of $AgSb_{0.94}Cd_{0.06}Te_2$ powder, thin films were prepared by the drop-casting method. All the films were dried at room temperature and annealed at 60 °C for 4 h. In this way, six composite thin film samples containing 0, 30, 50, 90, 95, and 97.5 wt.% of $AgSb_{0.94}Cd_{0.06}Te_2$ were prepared. At this stage, the films were cut into two halves, and one half of each film was hot pressed with the help of a two column lab press under a pressure load of 150 kN at 80 °C for 60 s, as depicted in the step 3 of Figure 1 and Figure S1 (Supporting Information) in the supporting information. The conditions for hot pressing were optimized by varying the temperature and duration of pressing, keeping the pressure at 150 kN. The optimized conditions of 80 °C and 60 s avoid cracking, peeling, etc. Above 80 °C, films exhibit signs of peeling off from the substrate.

The corresponding hot-pressed samples containing 0, 30, 50, 90, 95, and 97.5 wt.% of $AgSb_{0.94}Cd_{0.06}Te_2$ have been named as PEDOT:PSS, P1, P2, P3, P4, and P5. At the end of the fabrication process, easy-to-cut, dense, crack-free, bendable composite films were successfully obtained, and a picture of one of these samples containing a maximum amount of $AgSb_{0.94}Cd_{0.06}Te_2$ (P5, 97.5 wt.%) has been shown in step 4 of Figure 1. The chemical structure of PEDOT:PSS polymer, the unit cell for $AgSb_{0.94}Cd_{0.06}Te_2$, and the scanning electron microscope (SEM) image of PVDF substrate are given in Figure 1B,C, respectively. Cross-sectional backscattered SEM images of pressed and non-pressed P5 (Figure 1D) show that the PEDOT:PSS/$AgSb_{0.94}Cd_{0.06}Te_2$ composites form a uniform thin layer on PVDF substrates without impregnating it. Hot pressing decreases the thickness of the composite layer from 31.76 ± 0.40 to 24.07 ± 1.36 µm in the P5 sample. The thicknesses of all other compositions are given in **Table 1**. The PVDF membrane is also compressed down from 93.28 to 52.76 µm on average in all the samples.

2.2. Characterization of Composite Thin Films using SEM, UPS, and XRD

The surface morphologies of the PEDOT: PSS and composite films P1 to P5 were studied by scanning electron microscopy and are shown in **Figure 2**. The surface SEM images for the $AgSb_{0.94}Cd_{0.06}Te_2$ powder are provided in the supporting information (Figure S2, Supporting Information). It is found that PEDOT: PSS/$AgSb_{0.94}Cd_{0.06}Te_2$ composites form uniform films on PVDF substrates, and the surface roughness increases as the amount of $AgSb_{0.94}Cd_{0.06}Te_2$ increases.

The backscattered SEM images shown in the insets in Figure 2A and Figure S3 (Supporting Information) provide

Table 1. Sample names and composition, temperature, and thermoelectric parameters of pressed films.

Sample	$AgSb_{0.94}Cd_{0.06}Te_2$ [wt.%]	Temperature[a)] [°C]	σ [S cm^{-1}]	S [μV K^{-1}]	P.F [μW m^{-1} K^{-2}]
PEDOT: PSS	0.0	45.2 ± 2.50	2.2 ± 0.04	16.8 ± 0.45	0.07 ± 0.04
P1	30.0	45.8 ± 2.85	4.1 ± 0.12	18.1 ± 0.20	0.14 ± 0.01
P2	50.0	46.5 ± 2.75	0.9 ± 0.01	22.2 ± 1.40	0.05 ± 0.002
P3	90.0	42.6 ± 0.50	5.8 ± 0.05	148.0 ± 10.50	11.03 ± 0.02
P4	95.0	45.8 ± 2.01	8.9 ± 0.08	172.8 ± 1.57	26.62 ± 0.73
P5	97.5	43.5 ± 0.12	15.4 ± 0.19	185.9 ± 3.08	53.45 ± 2.40

[a)] The average sample temperature is taken from the actual temperature measurement of at least 3 independent samples.

useful information on the relative distribution of inorganic and organic phases in films. The brighter spots corresponding to heavier elements Ag, Sb, Cd, and Te were uniformly distributed, and their intensity increased with an increase in the amount of $AgSb_{0.94}Cd_{0.06}Te_2$ from P1 to P5. These backscattered images give information up to a penetration depth of ≈5μm, which was calculated using Monte Carlo simulations for PEDOT: PSS at 30 keV beam energy (Figure S4, Supporting Information). For information from higher penetration depths, element-specific energy dispersive X-ray spectroscopy (EDS) with a penetration depth of 15 μm was carried out on one of the samples, P2.

Figure 2C and the EDS spectrum in Figure S5 (Supporting Information) confirmed that Ag, Sb, Te, and S are homogeneously distributed throughout the sample, and no phase separation occurs. Figure 2B is the backscattered SEM image for P2 for the area scanned for EDS. After the surface characterization of the films, backscattered cross-sectional SEM was used to determine the thicknesses of the composite layer and the soft PVDF substrates. The absolute thicknesses were calculated by taking an average of at least 3 measurements along the cross-section. All the cross-sectional SEM images and the thicknesses of the respective layers have been provided in Figures S6–S17 (Supporting Information). Hot pressing significantly reduces the thicknesses of the composite material and the soft PVDF substrates. On average, the thickness of the PVDF substrate after pressing reduces from 93.28 to 52.76 μm, about a 43.44% decrease in the substrate thickness in all the samples.

Ultraviolet photoelectron spectroscopy (UPS) was used to study the energy levels of individual materials and the composite films in non-pressed samples (the samples could not be pressed

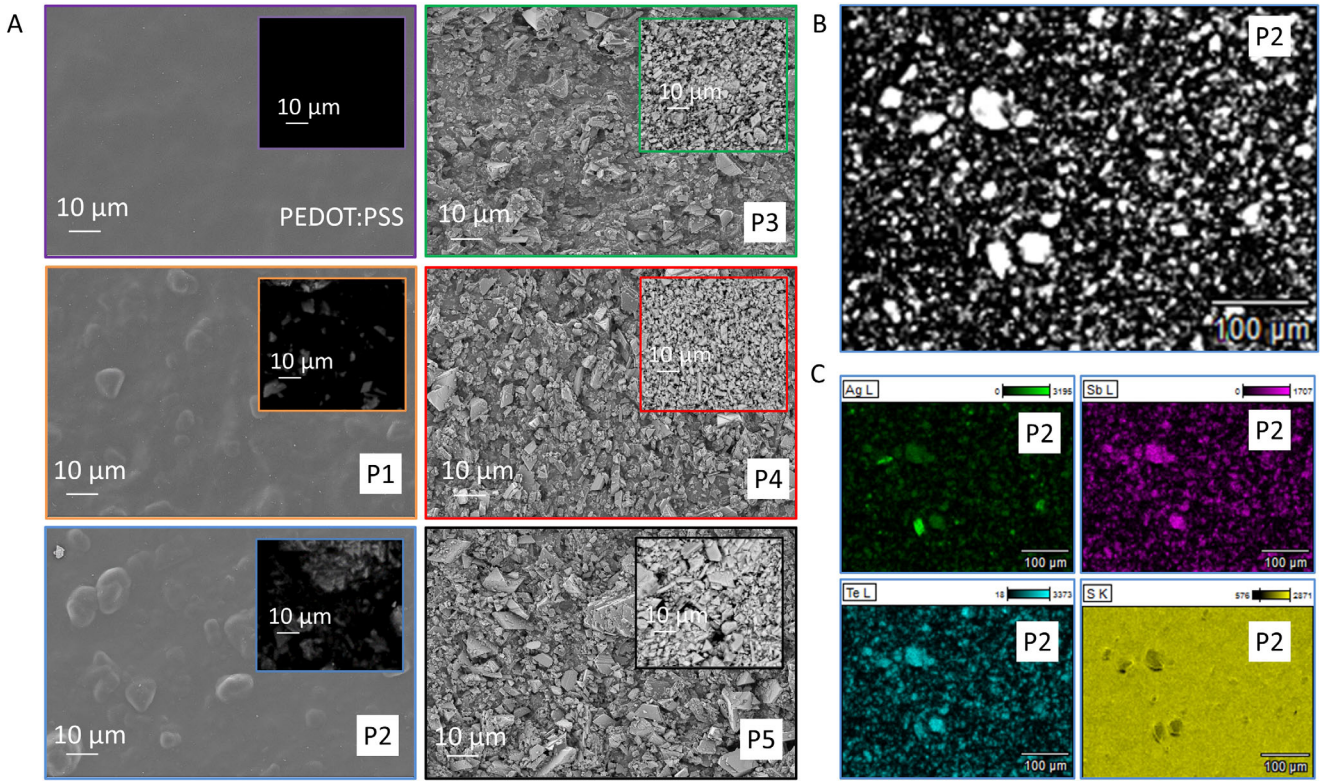

Figure 2. A) Surface scanning electron microscopy images of PEDOT:PSS (violet frame) and composite films P1(orange), P2(blue), P3(green), P4 (red), and P5(black) with backscattered electron images shown in the insets; B) Backscattered SEM and C) EDS elemental mapping for Ag, Sb, Te and S for P2 composite film.

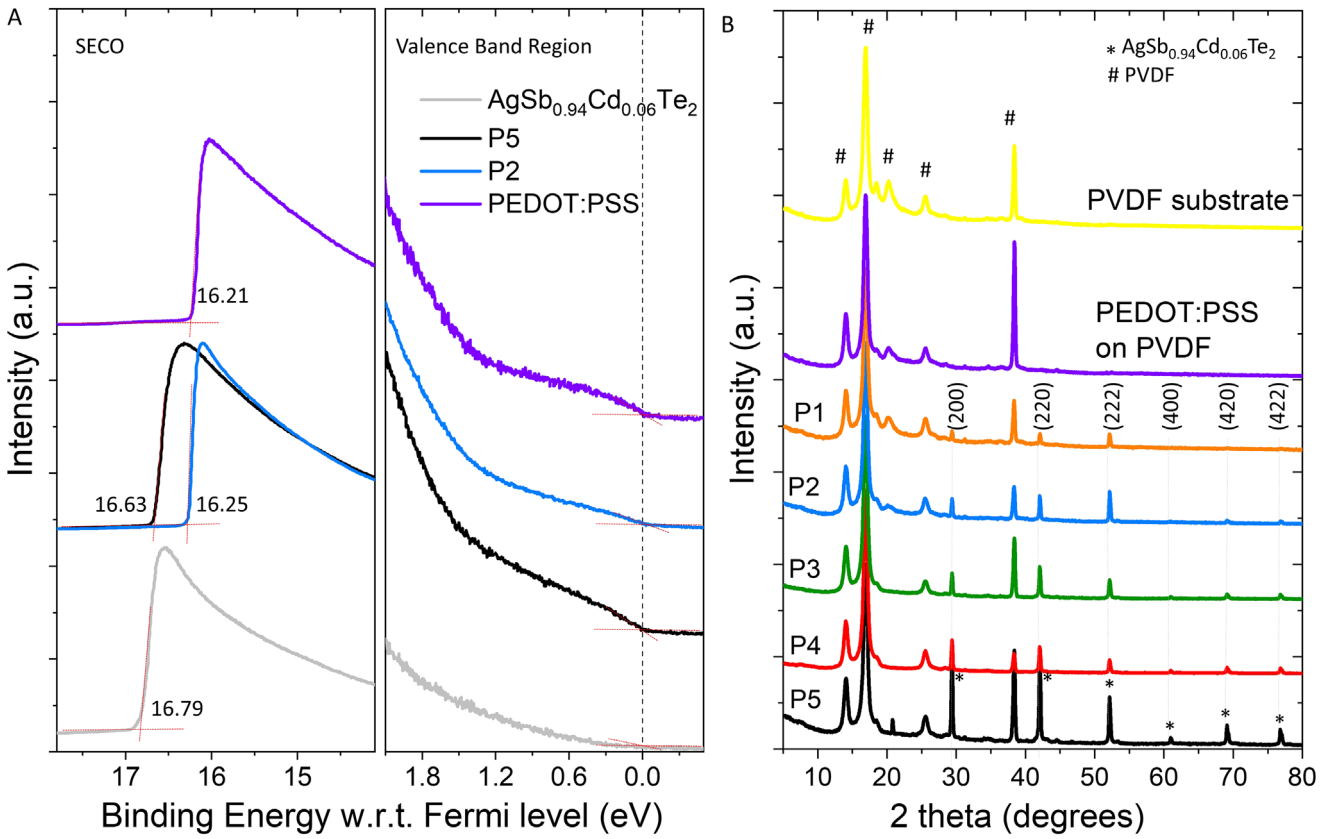

Figure 3. A) UPS spectra depicting the SECO and expanded valence band regions of PEDOT: PSS (violet), P2 (blue), P5 (black) coated on ITO substrates and $AgSb_{0.94}Cd_{0.06}Te_2$ (grey) measured as pellet; B) Wide angle X-ray diffraction patterns of PVDF substrate, PEDOT: PSS, P1, P2, P3, P4 and P5 composite films in the 2θ range 5°–80°.

due to the need for sample preparation on conducting glass substrates). The work function (φ)s and the ionization potential (IP)s of PEDOT: PSS (φ = 5.00 ± 0.16 eV, IP = 5.12 ± 0.02 eV) and $AgSb_{0.94}Cd_{0.06}Te_2$ (φ = 4.43 ± 0.11 eV, IP = 4.57 ± 0.01 eV) were calculated from secondary electron cutoff (SECO) and valence band edges with respect to the Fermi level as shown in the **Figure** 3A. The energy levels of P2 (φ = 4.97 ± 0.02eV, IP = 5.12 ± 0.01 eV) and P5 (φ = 4.58 ± 0.03 eV, IP = 4.68 ± 0.01 eV) resembled that of PEDOT: PSS and $AgSb_{0.94}Cd_{0.06}Te_2$, respectively. No modification in the density of states of individual materials due to blending was observed since the measured VB region of the pristine samples and the composites strongly resemble. Only the SECO for the composites shifts between those of the components as per the composition. All details of UPS measurements are explained in the Supporting Information. Thereby, the main contribution to the Seebeck coefficient comes from the inorganic counterpart only.

Wide-angle X-ray diffraction patterns of PVDF substrate, PEDOT:PSS, P1, P2, P3, P4, and P5 composite films have been shown in Figure 3B. PVDF, which is a semi-crystalline polymeric matrix, shows the characteristic diffraction peaks at 14.0°, 16.8°, 20.5°, 25.6°, and 38.4°.[25] The peaks at 2θ of 29.5°, 41.9°, 52.3°, 60.9°, 69.1° and 78.8° have been assigned to reflection planes $AgSb_{0.94}Cd_{0.06}Te_2$ (Fm-3m space group) from the diffraction peaks of powder $AgSb_{0.94}Cd_{0.06}Te_2$.[22] As is evident from Figure 3B, the intensity of these reflection peaks increases with increasing concentration of $AgSb_{0.94}Cd_{0.06}Te_2$ in the composite films, and the basic crystalline structure of the inorganic part was retained in all the composite films. Thus, the "electron-crystal" property of the inorganic component can be expected to be maintained in composite thin film systems.

2.3. Thermoelectric Properties, Charge Carrier Mobilities, and Charge Carrier Densities of the Composite Films

The details of the TE setup for determining the TE parameters are given in Figures S18–S20 (Supporting Information). The electrical conductivities, Seebeck coefficients, and power factors of all the films with respect to the amount of $AgSb_{0.94}Cd_{0.06}Te_2$ have been shown in **Figure** 4A,B and given in Table 1 and Table S1 (Supporting Information). In Figure 4A, initially, as the amount of $AgSb_{0.94}Cd_{0.06}Te_2$ in the films increases to 30 and 50 wt.% in P1 and P2, the TE properties of P1 (σ = 4.1 ± 0.12 S cm $^{-1}$, S = 18.1 ± 0.2 μV K $^{-1}$, P.F. = 0.14 ± 0.01 μW m^{-1} K^{-2}) and P2 (σ = 0.9 ± 0.01, S = 22.2 ± 1.4μVK $^{-1}$, P.F. = 0.05 ± 0.002 μW m^{-1} K^{-2}) were close to PEDOT: PSS (σ = 2.2 ± 0.04 S cm $^{-1}$, S = 16.8 ± 0.45 μVK $^{-1}$ and P.F. = 0.07 ± 0.04 μW m^{-1} K^{-2}). A similar behavior was observed for non-pressed films as shown in Figure 4B. As the amount of $AgSb_{0.94}Cd_{0.06}Te_2$ was further increased to 90.0, 95.0 and 97.5 wt.% in P3, P4 and P5, a unique simultaneous enhancement in the electrical conductivities and

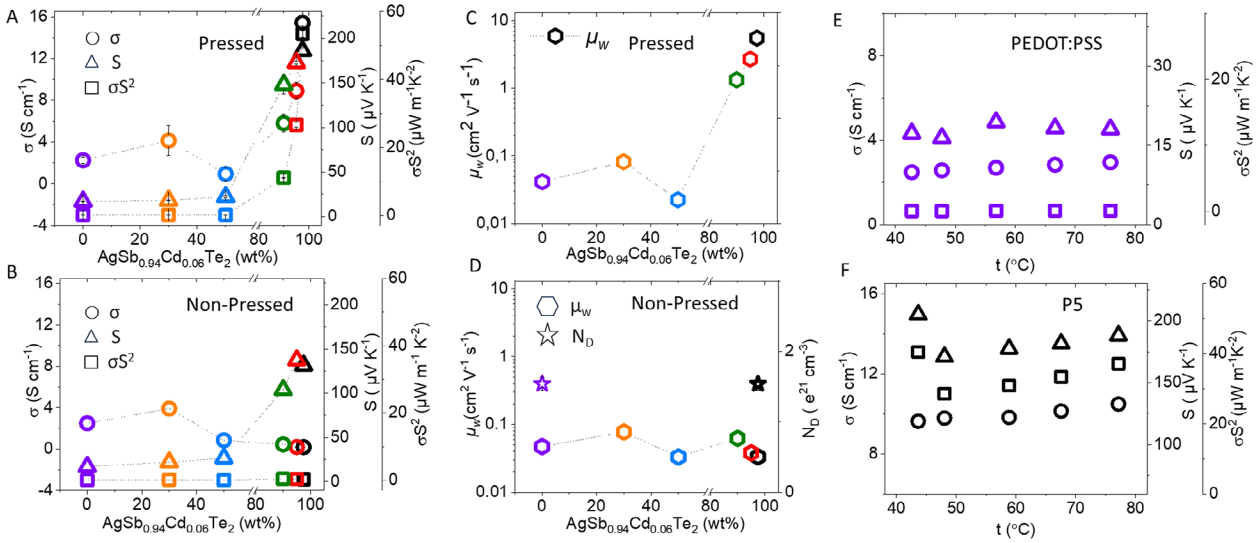

Figure 4. A,B) Electrical conductivity (○), Seebeck coefficient (Δ) and power factor (□), of PEDOT:PSS (violet), P1(orange), P2 (blue), P3 (green), P4 (red) and P5 (black) versus amount of $AgSb_{0.94}Cd_{0.06}Te_2$; C,D) Weighted carrier mobilities (⬡) and carrier densities (★) versus amount of $AgSb_{0.94}Cd_{0.06}Te_2$; E,F) Temperature dependent TE properties of PEDOT:PSS and P5, respectively.

Seebeck coefficients was observed along the whole regime with increasing amount of $AgSb_{0.94}Cd_{0.06}Te_2$ in P3 ($\sigma = 5.8 \pm 0.05$ S cm^{-1}, S = 148.00 ± 10.5 μV K^{-1},), P4 ($\sigma = 8.9 \pm 0.08$ S cm^{-1}, S = 172.80 ± 1.57 μV K^{-1}) and P5 ($\sigma = 15.4$ S cm^{-1}, S = 185.9 ± 3.08 μV K^{-1}). Highest Seebeck coefficients up to 204.9 μV K^{-1}, average Seebeck of 185.9 μV K^{-1}, and average power factor of 53.45 μW m^{-1} K^{-2} were obtained for P5. The electrical conductivities for the non-pressed films remained uniformly low, as seen in Figure 4B. This simultaneous increase in the S and σ with increasing concentration of Cd-doped $AgSbTe_2$ could be attributed to the high S of $AgSbTe_2$ due to the high effective mass of the hole and a smooth conduction of the hole through the inorganic Cd-doped $AgSbTe_2$.

In most of the previous works based on PEDOT: PSS composites, irrespective of the improvement in the electrical conductivities, the Seebeck coefficients of the composite films remained low around the Seebeck coefficient of the pristine PEDOT: PSS (16–22 μV K^{-1}), resulting in the overall low power factors except for the report using high Seebeck SnSe inorganic component.[18b] Our PEDOT: PSS/$AgSb_{0.94}Cd_{0.06}Te_2$ composite thin films on PVDF exhibit a high Seebeck coefficient (S≈205 μV K^{-1}) and approach the values of the inorganic TE material used (S ≈ 248 μV K^{-1} in highly densified pellet). Our observations indicate that high amounts of inorganic TE materials (90 wt.% and above) are needed to significantly improve the Seebeck coefficients of the composite films. For our PEDOT: PSS/$AgSb_{0.94}Cd_{0.06}Te_2$ composite system, robust, flexible composite films could be prepared with PEDOT: PSS concentration as low as 2.5 wt.%, below which the films became fragile and difficult to handle. Additionally, the TE properties and mechanical stability of the thin films upon bending of the thin film were investigated (Table S2, Supporting Information). Even though the electrical conductivity decreases after bending, there is only a negligible decrease in the Seebeck coefficient, even after 160° bending of the film. Accordingly, the PF decreased from 17.66 (for 49° bending) to 14.3 μW m^{-1} K^{-2} (for 160° bending). No cracks or delamination could be observed even after 160° bending of the films in SEM measurements (Figure S21, Supporting Information). Additional cycles of bending carried out at a fixed angle of bending at 49° show that the electrical conductivity remains the same for the repeated cycles after a first drop in initial conductivity due to storage of samples for ≈2 months under air (Table S3, Supporting Information). Even though storage under ambient conditions shows a decrease in conductivity, storage in a glovebox does not change the TE properties. Even though no noticeable morphological changes could not be detected in SEM after bending, the fact that the electrical conductivity (and consequently PF) decreases indicates that the connectivity and percolation via the inorganic phase may be decreasing on bending as well as during storage under air. Nevertheless, we assume that substantial mechanical stability at high inorganic content was achieved due to the improved adhesion of the composite onto the porous PVDF membrane used.

To investigate what led to an increase in conductivity with increasing amount of $AgSb_{0.94}Cd_{0.06}Te_2$, the weighted charge carrier mobilities in pressed and non-pressed films were determined and plotted in Figure 4C,D, respectively. The weighted mobilities, which reflect hole mobility weighted by the density of electronic states, were calculated from Seebeck coefficients and electrical resistivity measurements using the following equation suggested by Snyder et al.[26] The relationship given in Equation (3) has been suggested for good results at room temperature and above, and is valid for charge carrier mobilities as low as 10^{-3} cm^2 V^{-1} s^{-1}:

$$\mu_w = 331 \frac{cm^2}{Vs}\left(\frac{m\Omega cm}{\rho}\right)\left(\frac{T}{300K}\right)^{-3/2}\left[\frac{exp\left[\frac{|S|}{k_B/e}-2\right]}{1+exp\left[-5\left(\frac{|S|}{k_B/e}-1\right)\right]}+\frac{\frac{3}{\pi^2}\frac{|S|}{k_B/e}}{1+exp\left[5\left(\frac{|S|}{k_B/e}-1\right)\right]}\right] \quad (3)$$

Here, μ_w is the weighted mobility, ρ is the electrical resistivity measured in mΩ cm, T is the absolute temperature in K, S is the Seebeck coefficient, and $k_B/e = 86.3\ \mu V\ K^{-1}$.

The weighted mobilities for the composite films increased continuously and rapidly as compared to PEDOT: PSS, which showed a weighted mobility of 0.042 $cm^2\ V^{-1}\ s^{-1}$. The composite film P3 showed a remarkable 30 times higher charge carrier mobility (1.36 $cm^2\ V^{-1}\ s^{-1}$), whereas the charge carrier mobilities for P4 (2.69 $cm^2\ V^{-1}\ s^{-1}$) is 60 times and for P5 (5.49 $cm^2\ V^{-1}\ s^{-1}$) is 150 times as high as PEDOT:PSS. A comparison with the corresponding non-pressed films in Figure 4D showed that carrier mobilities remain almost unchanged for the non-pressed samples. The determined weighted carrier mobilities of all the films have been provided in the supporting information in Tables S4 and S5 (Supporting Information). To get an insight into the charge transport mechanisms, charge carrier concentration (N_D) was measured for PEDOT:PSS and the films containing 97.5 wt.% of $AgSb_{0.94}Cd_{0.06}Te_2$ by Mott–Schottky measurements on metal-insulator-semiconductor (MIS) devices and is given in Figure 4D.

The details of the device preparation method, schematic cross-section of the MIS device, and all the details of charge carrier density (N_D) measurements have been given in the supporting information and Figure S22 (Supporting Information). The charge carrier density N_D was extracted as the slope of a linear fit in the depletion regime of the plot of $\frac{1}{C_{tot}^2}$ against the applied bias voltage V_{Bias}, whereas the extrapolated x-intercept gave the flat band voltage V_{Fb} (see SI for details). PEDOT: PSS exhibited a carrier density of 1.63 $e^{21} \pm 0.09\ e^{21}\ cm^{-3}$ as an average over 5 working devices. P5 showed a similar carrier density of 1.54 $e^{21} \pm 0.09e^{21}$ cm^{-3} obtained as average of 3 working devices. These values suggest that no change in the density of charges occurs in the non-pressed films, even if a high concentration of inorganic material is present.

To understand the effect of temperature dependence on charge transport, thermoelectric properties were measured in the temperature range from 40 to 80 °C, as shown in Figure 4E,F for PEDOT: PSS and P5, respectively. The temperature-dependent TE properties of all the other samples have been given in Figure S23 (Supporting Information). As seen in Figure 4E, the electrical conductivity of PEDOT: PSS increases linearly with an increase in temperature, confirming the semiconducting behavior of the film and transport through a hopping process, as known for PEDOT: PSS.[27] The temperature-dependent conductivity of the P5 composite films also shows a positive slope with a linear increase in the conductivity. Although the Seebeck coefficient decreases initially from 205μV K^{-1} (at 43.6 °C) to 171μV K^{-1} (at 48.0 °C), a slight increase is observed with an increase in the temperature afterward. All the composite films showed positive Seebeck coefficients, indicating p-type behavior and a slight increase in S at higher temperatures.

3. Conclusion

We have successfully fabricated mechanically stable flexible composite TE thin films based on PEDOT: PSS and $AgSb_{0.94}Cd_{0.06}Te_2$, containing 0, 30, 50, 90, 95, to 97.5 wt.% $AgSb_{0.94}Cd_{0.06}Te_2$. Backscattered SEM images showed that all the composite films were dense, crack-free, and $AgSb_{0.94}Cd_{0.06}Te_2$ was homogeneously distributed without any phase separation. A simultaneous enhancement in the electrical conductivities and Seebeck coefficients was observed with an increasing amount of $AgSb_{0.94}Cd_{0.06}Te_2$ along the whole composition regime. We found out that the high Seebeck coefficient of $AgSb_{0.94}Cd_{0.06}Te_2$ (≈248 $\mu V\ K^{-1}$) could not be observed in the composite films containing less than 90 wt.% of $AgSb_{0.94}Cd_{0.06}Te_2$. A high Seebeck coefficient of 204.9 $\mu V\ K^{-1}$ and the highest power factor of 53.45 $\mu W\ m^{-1}\ K^{-2}$ were obtained for 97.5 wt.% of $AgSb_{0.94}Cd_{0.06}Te_2$ ≈40 °C. To understand the transport mechanisms, the energy levels of composite films were studied with ultraviolet photoelectron spectroscopy. The energy levels of P2 with 50 wt.% inorganic content resembled that of PEDOT: PSS ($\varphi = 5.00 \pm 0.16$ eV, IP = 5.12 ± 0.02 eV) and P5 containing 97.5 wt.% of $AgSb_{0.94}Cd_{0.06}Te_2$ resembled the pure inorganic $AgSb_{0.94}Cd_{0.06}Te_2$ ($\varphi = 4.43 \pm 0.11$ eV, IP = 4.57 ± 0.01 eV). Hence, no modification in the orbital energies was observed in the PEDOT:PSS/$AgSb_{0.94}$ $Cd_{0.06}Te_2$ composite system other than approaching the values of the respective components. Based on Mott–Schottky measurements, temperature dependent TE properties and calculation of weighted mobilities, we concluded that increase in weighted mobilty from PEDOT:PSS (0.042 $cm^2\ V^{-1}\ s^{-1}$) to P5 (5.491 $cm^2\ V^{-1}\ s^{-1}$) resulted in gradual increase in the electrical conductivity as the amount of $AgSb_{0.94}$ $Cd_{0.06}Te_2$ was increased. The composite on a porous membrane result in a flexible and efficient thin film. On bending and storage of these thin films, a loss in electrical conductivity was observed. In summary, we have demonstrated that blending of conducting polymers with suitable inorganic TE materials can provide an innovative way to efficient flexible TE materials approaching/achieving the Seebeck value of the inorganic compound used in thin films. By blending more than 90% of the inorganic compound, we achieved 80% of the Seebeck of the pure inorganic component.

4. Experimental Section

Materials and Preparation of Thin, Flexible Composite Films on PVDF Substrates: PEDOT: PSS (Clevios PH 1000) was purchased from Heraeus and used without further purification. High quality polycrystalline ingots (≈9 g) of $AgSb_{0.94}Cd_{0.06}Te_2$ were synthesized by mixing appropriate ratios of high purity starting materials, silver shots (Ag, Sigma–Aldrich 99.999%), antimony shots (Sb, Alfa Aesar 99.9999%), cadmium powder (Cd, Sigma–Aldrich 99.5%) and tellurium shots (Te, Alfa Aesar 99.999+ %) in quartz tubes. The tubes were sealed under vacuum (≈10^{-5} Torr) and slowly heated to 673 K over 12 h, then heated up to 1123 K in 4 h followed by soaking for 10 h, and then slowly cooled down to room temperature over a period of 20 h.[22] The ingots were ground into fine powders and used in the composite films. The size distribution of the particles was confirmed by SEM (0.25–20 μm) and is given in Figure S2 (Supporting Information). The thin films containing 0, 30, and 50 wt.% of $AgSb_{0.94}Cd_{0.06}Te_2$ were prepared by the drop-casting method. Films containing 90, 95, and 97.5 wt.% of $AgSb_{0.94}Cd_{0.06}Te_2$ were prepared by doctor blading the slurry on PVDF substrates. A two-column lab press P/O/Weber PW 20 GS, assisted with a temperature control unit under a pressure load (system ram force) of 150 kN at 80 °C, was used to hot press the film.

Scanning Electron Microscopy: The surface and cross-sectional SEM was done by using a ZEISS Ultra Plus field emission scanning electron microscope using in-lens, secondary electron, and in-lens energy-selective backscatter detectors. For cross-sectional analysis, surfaces were prepared by cryo-freezing the thin films and breaking them to prevent any smearing of deposited layers. The corresponding elemental mapping and energy dispersive X-ray spectroscopy (EDS) was done by Zeiss LEO 1530. Before

carrying out the SEM analysis, all the samples were coated with a layer of platinum using a Leica EM ACE600 sputter coater.

Ultraviolet Photoelectron Spectroscopy: UPS measurements were carried out on a PHI 5000 Versa Probe III system equipped with a He discharge UV light source providing stable and continuous He I and He II lines, under ultrahigh vacuum ($\approx 10^{-9}$ mbar). Samples for UPS measurements were obtained by doctor blading a thin film of P2 and P5 on ITO-coated glass substrates. PEDOT: PSS film was deposited by the drop-casting method. For pure $AgSb_{0.94}Cd_{0.06}Te_2$, 269.42 mg of the powder was pressed, and a 0.5 mm thick pellet was obtained using a lab press at room temperature. The samples were transferred to the main chamber of the spectrophotometer, and a He I source (55 W) was used to eject photoelectrons. The ejected photoelectrons were collected at a 90° take-off angle by using a multichannel semi-spherical analyzer. A bias voltage of −5V was applied to the sample stage (between the substrate and the analyzer) for measuring both the valence band maximum (VBM) and secondary electron cutoff (SECO) signals. Both SECO and VBM spectra were collected from at least 3 different areas in two to three different samples, and only the reproducible measurements were considered for further calculations. The VBM and SECO binding energy values necessary to determine ionization potential and work function, respectively, were obtained by the linear extrapolation method. The Fermi level E_F of all the samples was referenced to the Fermi level of polycrystalline Au foil after Ag+ sputter-cleaning for 5 min. The energy resolution of the VBM and SECO is 0.16 eV, i.e., the instrument error was derived from the full-width half-maximum of the Au Fermi edge.

Wide-Angle X-Ray Analysis: Wide-angle X-ray diffraction patterns of all the films were recorded using a Bruker D8 Advance diffractometer with a copper target. The Spectra were recorded using Cu Kα radiation in the range of $2\theta = 5°$–$80°$.

Thermoelectric Characterization: The electrical conductivity and Seebeck coefficient measurements were performed with ADVANCE RIKO's Seebeck coefficient/electric resistance measurement system (ZEM-3) in a Helium atmosphere at −0.05 MPa. Thin composite films were mounted on a thin film sample holder made of alumina and having two Ni electrode plates screwed at the two far ends of the holder. The films were placed under the Ni plates onto the alumina holder and contacted with the help of silver paste. The films on the sample holder were then sandwiched between two electrodes on the upper and lower blocks of the measurement setup (ULVAC-ZEM 3). The lower block was equipped with a heater to heat the sample at the lower end. The sample resistance value "R" is measured by measuring the current (I) set with the current power supply and the voltage (V) between probe A and probe B using the 4-terminal method. Seebeck coefficients were measured by measuring the temperature and voltages by Probe A and Probe B at the two contact points on the surface of the sample.

Charge Carrier Density (N_D) Measurements—Mott–Schottky Analysis: TEC-7 (FTO, 18.7 × 18.7 × 2.2 mm), 6–8 Ω/square, ≈500 nm FTO on glass) substrates were etched with dilute HCl/Zn-dust. After obtaining the etched electrode pattern, the substrates were brushed manually with sodium dodecyl sulfate and deionized water, followed by ultrasonication in 2 vol.% aqueous Hellmanex-III solution, water, acetone, and isopropanol. The substrates were blown dry with nitrogen and pre-treated with O_3/UV for 15 min at 50 °C. 170 nm of Al_2O_3 were deposited on the FTO-electrodes using ALD (H_2O/Al $(CH_3)_3$, 15 ms pulse duration, 150 °C, 5 s purge time, 2000 cycles), while leaving areas insulator-free for contacting the device during measurements. The substrates were immersed in a solution of *n*-octadecyltrichlorosilane (ODTS) in toluene (10 mmol L^{-1}) for 45 min at 60 °C in air to cap surface oxide groups. After SAM-formation, the substrates were rinsed with hexane, followed by ultrasonication in acetone and isopropanol to remove excess ODTS and blown dry with nitrogen. To deposit the semiconducting layer, PEDOT: PSS (Clevious PH 1000, shaken well in a Vortex shaker, and filtered through a syringe filter with GF 1–2 µm pore size) was drop-cast on top of the insulator layer, dried at RT and then at 60 °C. For the MIS device with a composite semiconducting layer, a composition containing the highest wt.% of $AgSb_{0.94}Cd_{0.06}Te_2$ (98.5 wt.%) in PEDOT: PSS was selected. 100 mg of $AgSb_{0.94}Cd_{0.06}Te_2$ powder and filtered PEDOT: PSS (2.57 mg, 0.217 mL) were ground well together in a mortar by hand with the help of a pestle. Once a smooth consistency was achieved, a thin composite semiconductor film was doctor-bladed on the insulator layer. Finally, Au electrodes were thermally evaporated using a shadow mask (d_{Au} = 70 nm).

Supporting Information

Supporting Information is available from the Wiley Online Library or from the author.

Acknowledgements

Bavarian State Ministry for Education, Science, and the Arts (Project: SolTech) is acknowledged for financial support. Also, the XPS/UPS facility (PHI 5000 Versa Probe III system) at Keylab Device Engineering in Bavarian Polymer Institute, University of Bayreuth, is acknowledged. Dr. Ulrich Mansfeld (Keylab Electron and Optical Microscopy, BPI) and Mrs. Martina Hyder are greatly acknowledged for knowledge sharing, discussions, and for support in SEM measurements. K.B. acknowledges support from the Swarna-Jayanti fellowship grant, Science and Engineering Research Board (SERB) (SB/SJF/2019-20/06), India. A. B. thanks CSIR, India for the fellowship.

Conflict of Interest

The authors declare no conflict of interest.

Data Availability Statement

The data that support the findings of this study are available from the corresponding author upon reasonable request.

Keywords

Cd doped $AgSbTe_2$, composite thermoelectric materials, poly(3,4-ethylenedioxythiophene) polystyrene sulfonate, thin film flexible thermoelectrics

Received: February 14, 2025
Revised: April 29, 2025
Published online: May 27, 2025

[1] Y. Wang, L. Yang, X.-L. Shi, X. Shi, L. Chen, M. S. Dargusch, J. Zou, Z.-G. Chen, *Adv. Mater.* **2019**, *31*, 1807916.
[2] S. Yang, P. Qiu, L. Chen, X. Shi, *Small Sci.* **2021**, *1*, 2100005.
[3] M. Kemerink, C. Müller, M. L. Chabinyc, M. Brinkmann, *Appl. Phys. Lett.* **2021**, *119*, 260401.
[4] J. Liang, S. Yin, C. Wan, *Annu. Rev. Mater. Res.* **2020**, *50*, 319.
[5] S. Ghosh, in *Conjugated Polymer Nanostructures for Energy Conversion and Storage Applications*, Wiley-VCH, Weinheim, Germany **2021**.
[6] H. Yan, N. Sada, N. Toshima, *J. Therm. Anal. Calorim.* **2002**, *69*, 881.
[7] A. J. Heeger, *Angew. Chem. Int. Ed.* **2001**, *40*, 2591.
[8] W. Zhao, J. Ding, Y. Zou, C. Di, D. Zhu, *Chem. Soc. Rev.* **2020**, *49*, 7210.
[9] G. H. Slack, in *Handbook of Thermoelectrics* (Ed: D. M. Rowe), CRC Press, New York, USA **1995**.
[10] J. Sun, M.-L. Yeh, B. J. Jung, B. Zhang, J. Feser, A. Majumdar, H. E. Katz, *Macromolecules* **2010**, *43*, 2897.
[11] H. Li, E. Plunkett, Z. Cai, B. Qiu, T. Wei, H. Chen, S. M. Thon, D. H. Reich, L. Chen, H. E. Katz, *Adv. Electron. Mater.* **2019**, *5*, 1800618.

[12] G. Zuo, X. Liu, M. Fahlman, M. Kemerink, *Adv. Funct. Mater.* **2018**, *28*, 1703280.
[13] R. M. W. Wolfe, A. K. Menon, T. R. Fletcher, S. R. Marder, J. R. Reynolds, S. K. Yee, *Adv. Funct. Mater.* **2018**, *28*, 1803275.
[14] H. Li, J. Song, J. Xiao, L. Wu, H. E. Katz, L. Chen, *Adv. Funct. Mater.* **2020**, *30*, 2004378.
[15] N. Saxena, J. Keilhofer, A. K. Maurya, G. Fortunato, J. Overbeck, P. M. Buschbaum, *ACS Appl. Energy Mater.* **2018**, *1*, 336.
[16] S. Xu, M. Hong, X.-L. Shi, Y. Wang, L. Ge, Y. Bai, L. Wang, M. Dargusch, J. Zou, Z.-G. Chen, *Chem. Mater.* **2019**, *31*, 5238
[17] W. Zheng, P. Bi, H. Kang, W. Wei, F. Liu, J. Shi, L. Peng, Z. Wang, R. Xiong, *Appl. Phys. Lett.* **2014**, *105*, 023901.
[18] a) K. Wei, T. Stedman, Z.-H. Ge, L. M. Woods, G. S. Nolasa, *Appl. Phys. Lett.* **2015**,*107*, 153301; b) H. Ju, J. Kim, *ACS Nano* **2016**, *10*, 5730.
[19] H. Song, C. Liu, H. Zhu, F. Kong, B. Lu, J. Xu, J. Wang, F. Zhao, *J. Electron. Mater.* **2013**, *42*, 1268.
[20] T. Zhang, K. Li, C. Li, S. Ma, H. H. Hng, L. Wei, *Adv. Electron. Mater.* **2017**, *3*, 1600554.
[21] Y. Wang, R. Chetty, Z. Liu, L. Wang, T. Ohsawa, W. Gao, T. Mori, *J. Mater. Chem. C* **2022**, *10*, 12610.
[22] S. Roychowdhury, T. Ghosh, R. Arora, M. Samanta, L. Xie, N. K. Singh, A. Soni, J. He, U. V. Waghmare, K. Biswas, *Science* **2021**, *371*, 722.
[23] R. Pathak, L. Xie, S. Das, T. Ghosh, A. Bhui, K. Dolui, D. Sanyal, J. He, K. Biswas, *Energy Environ. Sci.* **2023**, *16*, 3110.
[24] Y. Liu, M. Ibáñez, *Science* **2021**, *371*, 678.
[25] P. Martinsa, A. C. Lopesa, S. Lanceros-Mendez, *Prog. Polym. Sci.* **2014**, *39*, 683.
[26] G. J. Snyder, A. H. Snyder, M. Wood, R. Gurunathan, B. H. Snyder, C. Niu, *Adv. Mater.* **2020**, *32*, 2001537.
[27] A. M. Nardes, M. Kemerink, R. A. J. Janssen, *Phys. Rev.* **2007**, *76*, 085208.